Electroactive magnetic nanoparticles under magnetic attraction on a microchip electrochemical device

Feixiong Chen, Naoufel Haddour, Marie Frénéa-Robin, Yann Chevolot, Virginie Monnier

Electroactive magnetic nanoparticles under magnetic attraction on a microchip electrochemical device

Feixiong Chen[1], Naoufel Haddour[2], Marie Frenea-Robin[2], Yann Chevolot[1], Virginie Monnier[1]*

[1] *Université de Lyon, Ecole Centrale de Lyon, UMR CNRS 5270, Institut des Nanotechnologies de Lyon (INL), F-69130 Ecully Cedex, France.*

[2] *Université de Lyon, Ecole Centrale de Lyon, Université Claude Bernard, CNRS, Ampère, Ecully, F-69130, France*

*E-mail : virginie.monnier@ec-lyon.fr

Keywords : magnetic nanoparticles, ferrocenecarboxylic acid, magnetic field, surface-controlled process, diffusion-controlled process.

Abstract: This work focused on the introduction of electrochemical moieties (electroactive molecules) onto the surface of magnetic nanoparticles (NPs) based on carbodiimide coupling chemistry and the influence of magnetic attraction at the working electrode surface on their electrochemical behaviour. The magnetic NPs were first functionalized with polyamidoamine (PAMAM) dendrimer generation 0 and then with ferrocenecarboxylic acid (Fc) as electroactive molecule. Colorimetric titration, zeta potential measurements and infrared spectroscopy proved the effective conjugation of PAMAM and Fc onto NPs. The conjugation of Fc onto the NPs was also evidenced by voltammetry as it resulted in a half-peak potential shift from 0.328 V for free Fc to 0.590 V after coupling. A transition from a reversible to an irreversible behaviour was also observed. Finally, an external magnetic field was applied on Fc conjugated NPs to attract them onto the working electrode of a microchip electrochemical device, and the resulting modifications of the electrochemical behaviour were studied. Compared to Fc dispersed in

solution, the current peak height of Fc-conjugated NPs was 2-fold higher under magnetic attraction. The mechanism of electrochemical reaction was investigated and was found to be irreversible. Surprisingly, the reaction was diffusion-controlled upon attraction.

1. Introduction

Magnetic nanoparticles (NPs) have gained more and more attention in recent decades [1–3]. Indeed, NPs with magnetic properties can be used for separation and for recycling of catalysts or other functional solids [4,5]. They are also of particular interest in biomedicine and biotechnologies for bioseparation, hyperthermia, drug delivery and MRI [6]. To achieve this, magnetic NPs surfaces must be modified with appropriate materials or molecules in order to acquire sensing properties and targeting functions. For example, gold shell [7] modified magnetic NPs have been reported for Surface Plasmon Resonance bioassay amplification. The grafting of fluorophores [8], redox probes [9], oligonucleotides [10] or antibodies [11] have also been described. In particular, the introduction of electroactive molecules onto the surface of magnetic NPs is of great interest for the magnetic control of bioelectrocatalytic processes [12,13]. It is also a major issue for biosensing as electrochemical signal can be used for quantification while magnetic property can be used for separation and purification [14–16]. Ferrocene and its derivatives are good candidates as electroactive molecules due to their electrochemical reversibility, low oxidation potential, stable redox forms and their chemical inertia to oxygen [17]. Yet, only few studies report on their detailed electrochemical properties when immobilized onto magnetic NP surface [18–20] and on the influence of magnetic attraction of these ferrocene-NP conjugates near the working electrode on the electrochemical mechanism [12,21,22].

In this work, ferrocenecarboxylic acid (Fc) was immobilized onto magnetic NPs. First, carboxy-modified magnetic NPs were functionalized with polyamidoamine (PAMAM) dendrimer generation 0 using carbodiimide coupling chemistry [23,24]. The remaining free amine groups

were then used for Fc coupling. The different functionalization steps were followed by colorimetric titration, infrared spectroscopy and zeta potential measurements. Then, electrochemical characterizations were performed with a classical three-electrode cell and a microchip device. Using the microchip electrochemical device, it was possible to apply an external magnetic field to attract Fc-conjugated NPs onto the working electrode. The resulting electrochemical mechanism was then studied. The diffusion or surface-controlled character of the electrochemical reaction was compared between free Fc molecules, Fc-conjugated NPs dispersed in solution and Fc-conjugated NPs after magnetic attraction onto the working electrode surface.

2. Experimental

2.1. Materials

Carboxylate-modified magnetic NPs (300 nm diameter, 30 mg/mL, [COOH] = 10.5 µmol/mL) and activation buffer 10X were purchased from Ademtech. They are composed of a core containing superparamagnetic iron oxide NPs embedded in a COOH-modified polystyrene matrix. Ferrocenecarboxylic acid (Fc, ≥ 97%), ethylenediamine (EDA), polyamidoamine (PAMAM) dendrimers generation 0 (20 wt. % in methanol), phosphate buffered saline 0.01 M (PBS 1X, 0.0027 M potassium chloride and 0.138 M sodium chloride, pH=7.40 at 25ºC), (1-(3-(dimethylamino)propyl)-3-ethylcarbodiimide hydrochloride (EDC), N-hydroxysuccinimide (NHS) and Coomassie Brilliant Blue G (CBB) were purchased from Sigma-Aldrich. All chemicals were used without further purification. Milli-Q water (18.2 MΩ.cm) was used in all the preparations. SiC grinding paper for metallography P2500 was purchased from Buehler (France).

2.2. Surface modification of NPs

The surface modification of magnetic NPs was achieved according to a previously reported protocol [25].

2.2.1. Preparation of PAMAM-modified NPs (NPs@PAMAM)

5 µL of the initial carboxylate-modified NPs suspension were diluted in 500 µL of activation buffer 1X. Then, NPs were precipitated using a permanent magnet and washed once with the activation buffer 1X. After supernatant removal, NPs were redispersed in 500 µL of activation buffer 1X containing 12 µL of EDC (4 mg/mL, 0.02 mmol) and incubated for 2 hours at 37ºC under stirring at 550 rpm. After magnetic precipitation and supernatant removal, EDC-activated NPs were redispersed in 500 µL of activation buffer 1X containing 0.83 µL of PAMAM dendrimer generation 0. The molar ratios of [PAMAM]: [COOH from NPs] was set to 5. The NPs were incubated for 2 hours at 37ºC under stirring at 550 rpm. Finally, amino-functionalized NPs were washed once with activation buffer 1X stored at 4ºC before use.

1.2.2. Preparation of Fc-modified NPs (NPs@PAMAM@Fc)

5 mL of Fc solution (2.5 mM) prepared in PBS 1X were activated with 16 mg of EDC (0.08 mmol) and 11.7 mg of NHS (0.1 mmol) under magnetic stirring for 1 hour at room temperature. Then 1 mL of this solution was added to amine-modified NPs and incubated for 3 hours at 37ºC under stirring at 550 rpm. The Fc-modified NPs were washed twice with 1 mL of PBS 1X and stored at 4ºC before use.

2.3. Characterization methods

Infrared spectra were obtained in Attenuated Total Reflectance (ATR) mode on a diamond crystal using a Nicolet 6700 spectrometer from Thermo Scientific. Zeta potentials and hydrodynamic diameters were evaluated using a Zetasizer apparatus from Malvern Instruments. Ultraviolet-visible absorption spectra were collected in a quartz cell with a 1.0 cm path length

using a SAFAS-UV mc2 double-beam spectrophotometer. Each sample was measured three times to determine the mean values and standard deviations.

2.4. Colorimetric titration

2.4.1. Amine titration

The amine quantification of amine-modified NPs was achieved by Coomassie Blue titration method developed by Coussot *et al* [26]. Coomassie Brilliant Blue G (CBB) is a metachromatic dye used for a variety of histological staining. Thanks to the pH-dependent ionic interactions between SO_3^- groups from CBB molecules and NH_3^+ groups, the number of amine groups on the surface of NPs can be measured by UV-Visible absorption of CBB at 611 nm.

First, an acidic buffer (solution A) was prepared by mixing 85 mL of water with 10 mL of methanol and 5 mL of 99% acetic acid. Then a 58 µM CBB (solution B) was prepared by dissolving 2.5 mg of CBB in 5 mL of methanol and 45 mL of deionized water. A basic buffer (solution C) was prepared with 50 mL of a 1 M ammonia solution in water and 50 mL of methanol.

500 µL of NP dispersions (300 µg mL^{-1}) were precipitated under magnetic field and re-dispersed in 500 µL of solution A to protonate amine groups present at their surface. NPs were precipitated again and redispersed in 250 µL of solution B. After 15 min of vortexing, NPs were washed three times with solution A to remove the excess of CBB. They were subsequently redispersed in 250 µL of water to remove the acid buffer of solution A. Then, 200 µL of solution C was added to the NPs to deprotonate amines and release CBB molecules in solution. After 5 min of vortexing, NPs were precipitated under magnetic field and the UV-visible spectrum of resulting supernatant was recorded in a quartz cell with a 1.0 cm path length using a SAFAS-UV mc2 double-beam spectrophotometer. Solution C was used as a blank for each testing. Each sample was titrated three times to determine the mean values of NH_2 densities and standard deviations.

2.4.2. Carboxylic acid titration

The number of –COOH groups onto the NPs surface was determined by Toluidine Blue O (TBO) titration method, based on the electrostatic interaction between tertiary amine groups from TBO molecule and carboxylates.

NPs (300 µg mL^{-1}) were magnetically precipitated and the supernatant was removed. Next, the nanoparticles were incubated during 15 min at 40°C with 250 µL of a solution of TBO (1.14 mg/mL) in NaOH 1 mM. Then, the NPs were washed by successive washing/precipitation cycles in order to remove completely TBO molecules that did not interact with $–COO^-$ groups from nanoparticle surface. For each washing step, nanoparticles were incubated with NaOH 1 mM for 5 min at 40°C. Finally, nanoparticles were re-dispersed in 500 µL of 5% SDS solution in order to break interactions between $=N^+(CH_3)_2$ groups from the TBO and carboxylate groups from the nanoparticles. This solution containing TBO molecules was characterized by UV-Visible absorption spectroscopy at λ = 630 nm to deduce TBO concentration which was equal to the concentration of –COOH groups onto nanoparticle surface [27]. Molar extinction coefficient of TBO at 630 nm was found to be 26394 $L.mol^{-1}.cm^{-1}$.

2.5. Electrochemical measurements

2.5.1. Standard electrochemical cell

A conventional three-electrode cell was used, with bulk glassy carbon as working electrode (diameter: 4 mm, Origalys), saturated Ag/AgCl home-made electrode as reference and platinum as auxiliary electrode. PBS 1X buffer solution (pH = 7.4) was used as electrolyte.

2.5.2. Electrochemical microchip

A three-electrode microdevice system was based on screen-printed electrodes provided by PalmSens®. It consisted of electrodes printed on a plastic chip as shown in Figure 1a.

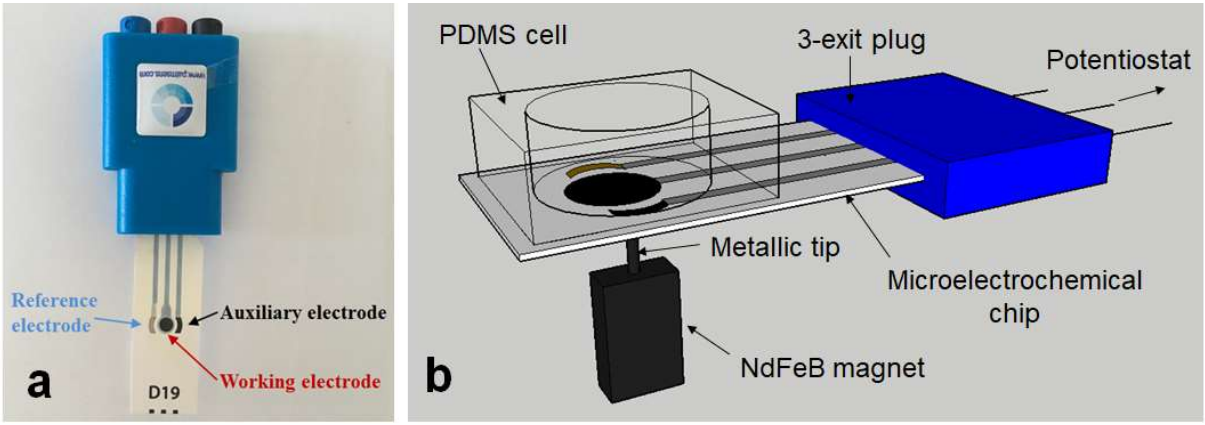

Figure 1. Photograph of the electrochemical microchip device (a) and set-up for electrochemical measurements under magnetic attraction (b).

The working electrode (0.04 cm^2) and auxiliary electrode were made up of carbon while the reference electrode was composed of silver (Ag/AgCl). The electrodes were connected to the potentiostat via a 3-exit plug. The electrochemical cell was created by polydimethylsiloxane (PDMS) embossing. A NdFeB magnet from Calamit company combined to a steel tip was used to concentrate the magnetic field on the working electrode (Figure 1b). The magnet dimensions were 40 mm x 20 mm x 10 mm while the tip length was 15 mm with a diameter of 2 mm and a narrowing to 1 mm for the last 5 mm. The tip was directly in contact with the microelectrochemical chip, thus the spacing distance between the tip end and the nanoparticles dispersion corresponds to the chip thickness, i.e. 200 µm. The magnetic field and magnetic field gradient at this distance from the tip were evaluated by simulation (Supporting Information, Figures S1 and S2), their values were 0.36 T and 600 T m^{-1}, respectively.

2.5.3. Data acquisition and analysis

Electrochemical measurements were performed with a OrigaStat-OGS080 potentiostat from OrigaLys using OrigaMaster 5 software for data acquisition and analysis. Cyclic voltammetry (CV) and square-wave voltammetry (SWV) experiments were conducted from 0 to 0.8 V at a

scan rate of 100 mV s^{-1}, a potential step of 10 mV, an amplitude modulation of 50 mV and a time modulation of 0.05 s. SWV technique offered the advantages to eliminate capacitive current coming from non-electroactive components, leading to a lower background signal. All SWV curves were obtained with dispersions at 300 µg of nanoparticles per mL. A linear fit was applied to eliminate the background signal.

3. Results and discussion

3.1 Preparation of NPs@PAMAM and NPs@PAMAM@Fc

The first functionalization step aimed at introducing amine groups at the surface of the initial carboxy-modified magnetic NPs. PAMAM generation 0 was selected as an amine crosslinker because it can provide large amounts of amine groups due to its dendrimeric structure [25]. PAMAM grafting onto the carboxylic acid groups of the magnetic NPs was performed using carbodiimide (EDC). The molar ratio [PAMAM]:[COOH] was set to 5. The number of amine groups after functionalization was evaluated by colorimetric titration with CBB. As displayed in Figure 2a, the initial COOH-modified NPs have a low background corresponding to an equivalent amine density of 0.30 ± 0.03 NH_2 groups per nm^2, which suggests a low level of nonspecific adsorption of CBB onto the initial carboxylated NPs. After PAMAM dendrimer generation 0 grafting, a density of 2.48 ± 0.21 NH_2 per nm^2 was measured onto the NP surface. This higher amine density compared to aminosilane-modified magnetic NPs [28] or to ethylenediamine-modified magnetic NPs [25] can be explained by the four amine groups on the PAMAM generation 0 dendrimers (Figure 2b). The number of remaining carboxylic groups onto magnetic NP surface after PAMAM grafting was also evaluated by TBO titration. The numbers of measured COOH groups onto the initial NPs and the PAMAM-modified NPs are given in Figure 2a.

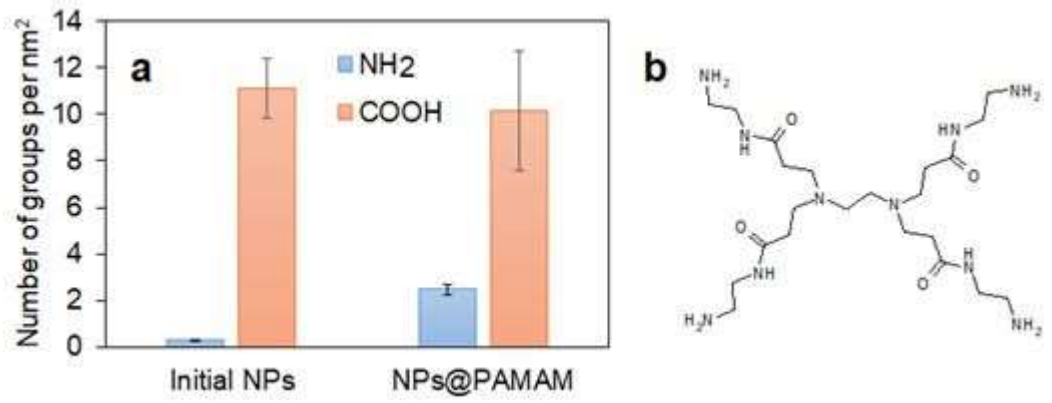

Figure 2. Number of NH_2 and COOH groups per nm^2 of initial and NPs@PAMAM determined by CBB titration and TBO titration, respectively (a) and chemical formula of PAMAM generation 0 (b).

This number seemed to decrease after PAMAM dendrimer grafting. Based on the number of COOH groups after and before PAMAM dendrimer grafting, PAMAM grafting yield was estimated to be around 5%. It indicated that after grafting, about 95% of COOH groups remained unreacted on the surface of magnetic NPs. The free amine groups at the surface of the magnetic NPs were then used for amide coupling of Fc. This second functionalization step was performed using NHS-ester chemistry. Zeta potentials and hydrodynamic volumes were measured at different pH at each step. Results are presented in Figure 3a.

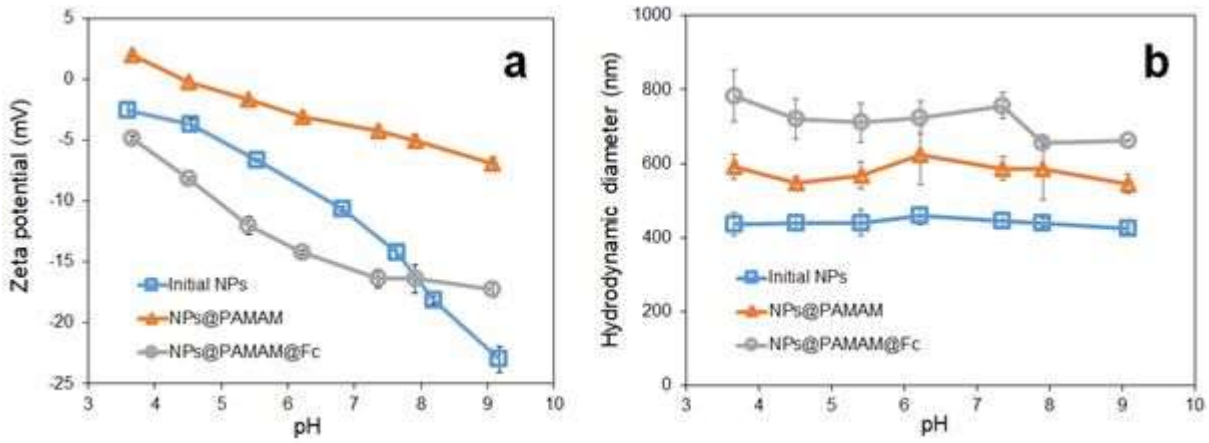

Figure 3. Zeta potentials (a) and hydrodynamic diameters (b) of initial NPs, NPs@PAMAM and NPs@PAMAM@Fc in phosphate buffer with different pH values.

Initial carboxy-modified nanoparticles were negatively charged over the whole studied pH range (from pH = 3.5 to pH = 9.5). After PAMAM grafting, the measured zeta potential increased for every tested pH. This increase of zeta potential may be attributed to the replacement of COOH by amine groups. Additionally, except at low pH, zeta potential values were still negative, probably because of the low coupling yield. After Fc conjugation, zeta potential decreased because some NH_2 groups were replaced by amide bonds between PAMAM and COOH groups from Fc. For the three types of nanoparticles, zeta potentials were mainly governed by the dissociation of the carboxylic groups into carboxylates. Consequently, increasing pH lead to more negative zeta potential. The hydrodynamic diameter of each NP type was evaluated by dynamic light scattering after each functionalization step (Figure 3b). An increase of hydrodynamic diameter from 400 to 600 nm was observed after PAMAM dendrimer grafting. The hydrodynamic diameter of NPs@PAMAM was further increased after Fc conjugation to around 800 nm. This could be attributed to NPs aggregation upon the successive functionalization steps. Nevertheless, as the hydrodynamic diameter was only doubled from initial to Fc-conjugated NPs, aggregates are supposed to be composed at the most of two NPs. The hydrodynamic diameters were not impacted by the pH whatever the type of

considered NPs (initial NPs, NPs@PAMAM, or NPs@PAMAM@Fc). The reason for this may be attributed to the fact that the zeta potentials were always negative over the studied pH range leading to repulsive ionic forces. Infrared spectroscopy was also used to characterize the NPs along the successive functionalization steps (Figure 4).

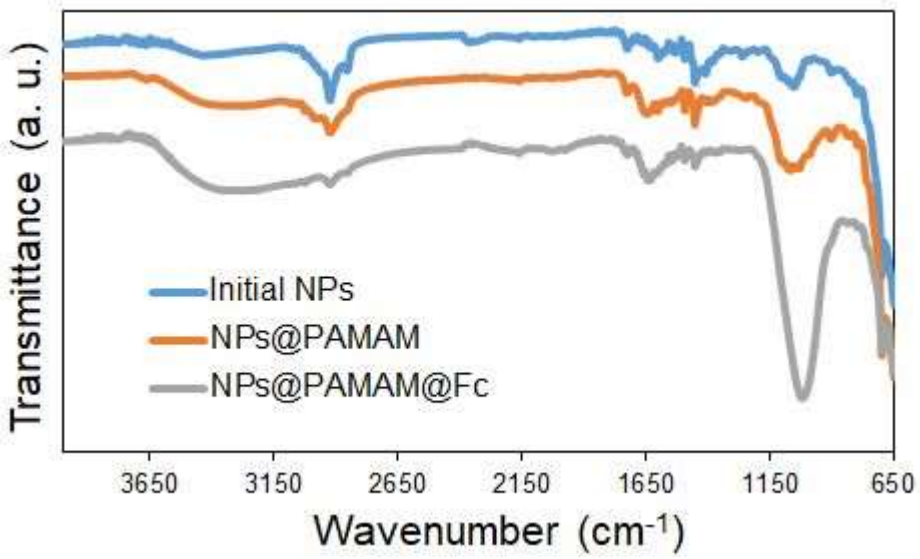

Figure 4. Infrared transmission spectra of initial NPs, NPs@PAMAM and NPs@PAMAM@Fc.

Initial carboxy-modified magnetic nanoparticle spectra exhibited many infrared peaks due to the presence of different chemical groups on NP surface. The peaks at 1730 cm^{-1} corresponded to the stretching vibrations of C=O from COOH groups. After PAMAM grafting, a new infrared peak located at 1650 cm^{-1} was observed and was attributed to the C=O stretching vibration originating from amide bond. Considering that there are 4 amide bonds per PAMAM generation 0 molecule (Figure 2b), its intensity may originate mainly from PAMAM dendrimer molecules and not from amide bonds formed between $-NH_2$ groups from PAMAM and -COOH groups from nanoparticles. After Fc conjugation, the peak of amide bond shifted to 1640 cm^{-1} while a new large band appeared at 1000 cm^{-1}. This band is related to the asymmetric vibration of C=C of cyclopentadienyl ring from ferrocene, implying that ferrocene was successfully grafted onto the surface of magnetic nanoparticles [12].

3.2 Electrochemical properties of NPs@PAMAM@Fc in solution

3.2.1 Oxidation peak

In order to validate the presence of Fc on the surface of NPs, the electrochemical properties of NPs@PAMAM@Fc were compared to that of NPs@PAMAM using a standard electrochemical cell. The measurements were performed using PBS 1X solution as electrolyte. Resulting CV and SWV data are presented in Figures 5a and 5b, respectively.

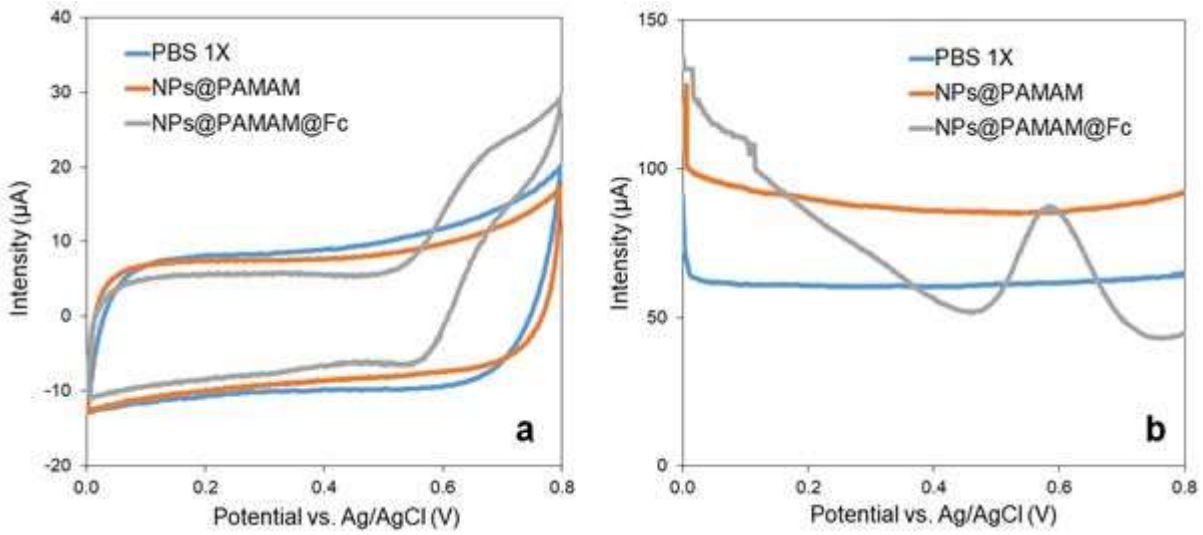

Figure 5. Electrochemical characterization of NPs@PAMAM and NPs@PAMAM@Fc: CV curves (a) and SWV curves (b) acquired from 0 to 0.8 V using a scan rate of 100 mV s^{-1}.

No oxidation nor reduction peaks were observed when measurements were performed in PBS 1X alone or with NPs@PAMAM. Capacitive currents were also similar. On the contrary, a significant electrochemical signal was detected for NPs@PAMAM@Fc using both CV and SWV. As shown in Figure 5a, CV curves show redox peaks characteristic of the Fe(III)/Fe(II) redox process. The oxidation and reduction peaks are located respectively at 0.636 and 0.544 V with a half-peak potential ($E_{1/2}$) at 0.590 V. Comparing this $E_{1/2}$ value with that of free Fc in the same electrolyte (0.328 V), it appears that the iron center in NPs@PAMAM@Fc is more difficult to oxidize. It is probably due to one or both following factors: (i) the substitution of

the oxygen atoms from COOH by the more electron-donating nitrogen atom from CONH can make the one-electron oxidation notably more difficult for this conjugated system. Due to electron-donating ability difference, this lead to the observed potential shift [21,22,29]; (ii) the dendritic effect of PAMAM shell that can generate a microenvironment hindering electron transfer between redox-active subunit and the electrode surface. It is well established that dendritic encapsulation of redox-active moieties alters their redox properties leading to an increase of their half-peak potential and to a decrease in their electrochemical reversibility [30,31].

3.2.2 Reversibility of the electrochemical reaction for free Fc molecules and NPs@PAMAM@Fc

From CV curves of free Fc molecules in solution and NPs@PAMAM@Fc obtained with a standard electrochemical cell (Figure S3, Supporting Information), in addition to the values of the cathodic peak potential E_{pc} and the anodic peak potential E_{pa}, the height of cathodic peak current i_{pc} and the height of anodic peak current i_{pa} were quantified. The results are listed in Table 1.

Sample	E_{pa} **(V)**	i_{pa} **(µA)**	E_{pc} **(V)**	i_{pc} **(µA)**	$\Delta E_p = \lvert E_{pc} - E_{pa} \rvert$ **(mV)**	I_{pa}/I_{pc}
Free Fc molecules	0.352	7.18	0.296	-6.90	64.5	1.02
NPs@PAMAM@Fc	0.636	3.40	0.544	-0.866	92.0	3.95

Table 1. Numerical data extracted from free Fc molecules and NPs@PAMAM@Fc CV curves obtained with the standard electrochemical cell from 0 to 0.8 V using a scan rate of 100 mV s^{-1} (Figure S3).

Calculations of $\Delta E_p = |E_{pc} - E_{pa}|$ and i_{pa}/i_{pc} can be used to evaluate the reversibility of the electrochemical process [25,26]. As shown in Table 1, ΔE_p for free Fc molecules in solution and NPs@PAMAM@Fc were 64.5 mV and 92.0 mV, respectively. These values were higher than 56.5 mV previously measured for a reversible system [26,27]. The value of i_{pa}/i_{pc} for free Fc

molecules in solution is close to the unity (1.02), which indicates a quasi-reversible system (i_{pa}/i_{pc} = 1). At the same time, the i_{pa}/i_{pc} value for NPs@PAMAM@Fc was 3.95, which was higher than the value obtained for a reversible system, indicating that the oxidation process of Fc when conjugated to NPs was irreversible. Therefore, it demonstrated that Fc molecules lost their reversibility to some extent, after conjugation onto NPs.

3.3 Influence of magnetic attraction of NPs@PAMAM@Fc onto working electrode using electrochemical microchip

3.3.1 Peak current intensity amplification

NPs@PAMAM@Fc can be easily actuated by an external magnetic field. Thus, using the electrochemical microchip described in the experimental section, the electrochemical properties of NPs@PAMAM@Fc dispersed in PBS 1X solution and NPs@PAMAM@Fc attracted onto the surface of working electrode were investigated. Figure 6a displays a photograph of the microchip before magnetic attraction: NPs@PAMAM@Fc are homogeneously dispersed in PBS 1X within the electrochemical cell as shown by the brown-orange appearance of the liquid.

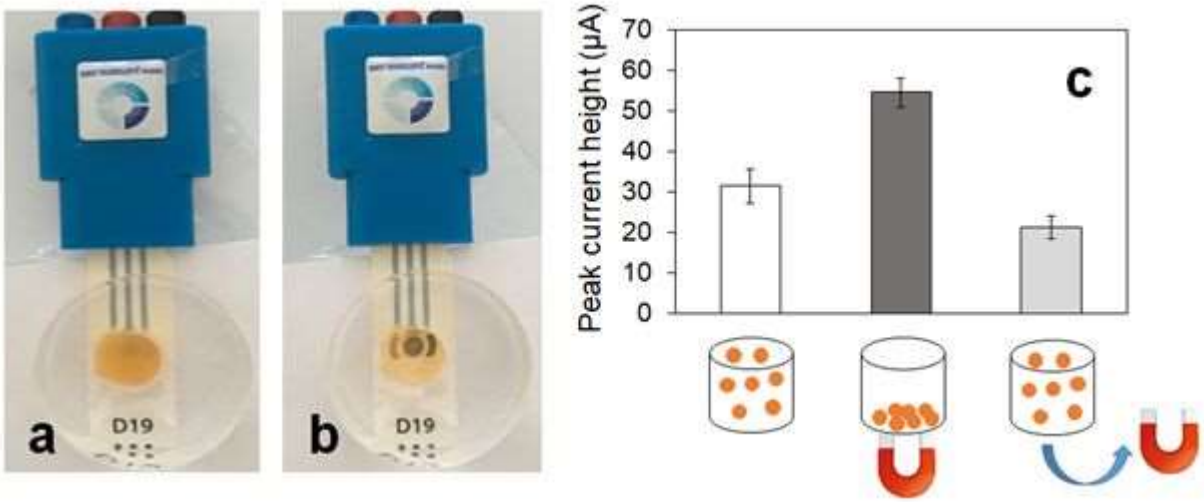

Figure 6. Photograph of the electrochemical microchip before (a) and after (b) magnetic attraction of NPs@PAMAM@Fc onto the working electrode. Peak current height measurement

extracted from SWV curves (c) obtained from 0 to 0.8 V with a scan rate of 100 mV s^{-1} for NP@PAMAM@Fc homogeneously dispersed in PBS 1X within the electrochemical cell (white bar), after magnetic attraction of the NPs onto the working electrode (dark grey bar) and after magnet removal (light grey bar). Each sample was measured three times to estimate the average values and standard deviations.

After magnetic attraction (Figure 6b), a brown-orange precipitate could be observed onto the central working electrode while the liquid became less coloured. This proved that almost all NPs@PAMAM@Fc were attracted on the surface of working electrode by the external magnetic field. Figure S4 (Supporting Information) shows the CV and SWV curves of NPs@PAMAM@Fc dispersed in solution and magnetically attracted on the working electrode. A nearly 1.5 fold increase of the electrochemical signal was obtained for magnetically attracted NPs@PAMAM@Fc compared to that of NPs@PAMAM@Fc freely distributed in the electrolyte. Figure 6c presented the height of peak currents for the two distribution states of NPs@PAMAM@Fc, and the height of peak current after removal of the NPs@PAMAM@Fc from the electrode by magnetic actuation. For dispersed NPs@PAMAM@Fc, the height of peak current was estimated to be 31.5 ± 4.1 µA. After attraction of NPs@PAMAM@Fc on the surface of the working electrode thanks to an external magnetic field, the height of peak current was increased to 54.6 ± 3.6 µA. After release of NPs@PAMAM@Fc from the working electrode following magnetic field cancellation, the height of peak current rapidly decreased to 21.3± 2.9 µA. These results are in agreement with the work of Lim *et al* [35], in which an iron-doped graphene oxide material was magnetically attracted or removed from electrode surface to modulate electrochemical processes. The measured current intensity was 2-fold higher when the material was magnetically attracted on the working electrode, which is in the same order of magnitude as our observations. This amplification can be explained as follows: an electrochemical reaction is a complex process in which the surface of the working electrode is

the main place where electrochemical reaction occurs. An electron flow takes place between the electrode and the electrolyte [33]. The electrochemical properties and concentration of electroactive molecules play important roles on electrochemical reaction. The electroactive species concentration close to the surface of the working electrode is also an important parameter. Figure S5 (Supporting Information) shows the influence of NPs@PAMAM@Fc concentration on the measured height of peak current for NPs dispersed in solution and magnetically attracted on working electrode. After magnetic attraction, surface concentration of NPs@PAMAM@Fc was increased, leading to a higher signal. Similar interpretation has already been proposed [22]. Nonetheless, by forcing the NPs to aggregate on the working electrode surface, one would expect to have a larger increase in the electrochemical signal. This could probably be attributed to the aggregation of NPs, when accumulated onto working electrode under magnetic attraction. In this situation, steric hindrance may limit the diffusion of counter ions between the electrolyte and the electrode.

3.3.2 Reversibility of the electrochemical reaction for free NPs@PAMAM@Fc and NPs@PAMAM@Fc magnetically attracted onto the working electrode

The reversibility of the electrochemical reaction was also investigated according to the data extracted from CV curves in the two states of distribution. The peak potential difference ΔE_p and peak current ratio i_{pa}/i_{pc} are summarized in Table 2.

Sample	$\Delta E_p = \lvert E_{pc} - E_{pa} \rvert$/mV	i_{pa}/i_{pc}
Free NPs@PAMAM@Fc in PBS 1X	75.5	1.70
NPs@PAMAM@Fc attracted on the working electrode	97.5	1.45

Table 2. Numerical data extracted from CV curves obtained with the electrochemical microchip from 0 to 0.8 V using a scan rate of 100 mV s^{-1} for free NPs@PAMAM@Fc in PBS 1X and NPs@PAMAM@Fc attracted on the working electrode (Figure S4).

Considering that ΔE_p for free and attracted NPs@PAMAM@Fc was respectively around 75.5 mV and 97.5 mV and that the peak current ratio i_{pa}/i_{pc} was higher than 1, the electrochemical reaction of NPs@PAMAM@Fc can be identified as an irreversible electrochemical process in both distribution states, which was expected according to results previously obtained in section 3.2.2 (Table 1). The different values previously obtained for ΔE_p and i_{pa}/i_{pc} using a standard electrochemical cell may be attributed to the difference of materials used for electrodes, the electrodes surfaces and the electrodes stability.

3.3.3 Determination of the diffusion- or surface-controlled character of the electrochemical reaction

The mechanism of electrochemical reaction was investigated. To this aim, the scan rate was varied allowing for the discrimination between diffusion dominant processes (diffusion-controlled) or interface-controlled reactions (surface-controlled). Generally, if the electron transfer at the working electrode surface is fast enough, the electrochemical reaction is limited by the diffusion process of redox species from the bulk of the solution to the electrode surface. In this case, the peak current intensity is proportional to the square root of the scan rate, as described by Cottrell equation [36,37]. On the contrary, if the peak current intensity is proportional to the scan rate (rather than square root of the scan rate), the electrochemical reaction is controlled by surface processes [38]. The effect of scan rate is based on the measurement of peak current intensity on CV curves at different scan rates. Correlation coefficient (R^2) of linear regression between peak current and scan rate or scan rate square root can be calculated to identify the mechanism of electrochemical reaction. The electrochemical reaction of Fc solution was investigated first, as a reference. Then, similar measurements were performed with NPs@PAMAM@Fc dispersed in PBS 1X solution or attracted on the surface of the working electrode. Figures S6, S7 and S8 (Supporting Information) show the CV curves of free Fc

molecule solution, free NPs@PAMAM@Fc dispersed in solution and NPs@PAMAM@Fc magnetically attracted onto the working electrode, respectively. Scan rates ranged from 100 mV s^{-1} to 2500 mV s^{-1}. The correlation coefficients extracted from these data are given in Table 3.

Sample	**Surface-controlled (*V*)**	**Diffusion-controlled ($V^{1/2}$)**
Free Fc molecules	0.9504	0.9977
Free NPs@PAMAM@Fc	0.9803	0.9703
NPs@PAMAM@Fc on working electrode	0.9562	0.9935

Table 3. Correlation coefficients (R^2) measured from height of peak current as a function of scan rate *V* and scan rate square root $V^{1/2}$ for free Fc molecules, free NPs@PAMAM@Fc and NPs@PAMAM@Fc attracted on the working electrode.

For free Fc molecules, the peak current increased with scan rate and was linear as a function of scan rate square root $V^{1/2}$ with a correlation coefficient R^2 = 0.9977, while the correlation coefficient was only of 0.9504, as a function of scan rate *V*. This indicated that the electrochemical reaction of Fc solution was a diffusion-controlled process [39]. For NPs@PAMAM@Fc dispersed in PBS 1X, the peak current intensity also increased with increasing scan rate, as obtained for Fc solution. However, the reduction peak of NPs@PAMAM@Fc almost disappeared at low scan rate (Figure S7, Supporting Information). Thus, only oxidation peak currents were used to investigate the mechanism of Fc electrochemical reaction. Linear regression of the peak current as a function of scan rate and as a function of scan rate square root gave similar correlation coefficients (0.9803 and 0.9703, respectively). Therefore, the reaction seemed to be controlled by both the diffusion- and surface reaction mechanisms [40,41]. Then, the influence of scan rate was also studied when NPs@PAMAM@Fc were magnetically attracted on the surface of the working electrode. The evolution of oxidation peak current height exhibited a higher correlation coefficient (R^2 =

0.9935) with the scan rate square root than with the scan rate (R^2 = 0.9562). It demonstrated that the electrochemical reaction of NPs@PAMAM@Fc attracted on the surface of working electrode was mainly controlled by diffusion. This result was unexpected since NPs were attracted on the electrode surface, thus Fc diffusion should not control the reaction mechanism. For NPs@PAMAM@Fc dispersed in electrolyte, the surface concentration of NPs depended on their diffusion and natural sedimentation onto the surface of working electrode. The size and stability of NPs strongly influenced their diffusion and the rate of natural sedimentation. As demonstrated previously, we managed to obtain NPs@PAMAM@Fc showing low aggregation and good dispersion in PBS 1X. Therefore, natural sedimentation of NPs@PAMAM@Fc was probably a slow process and resulted in a low surface concentration of NPs@PAMAM@Fc and consequently to a decrease of surface reaction rate. This may explain why in this case the reaction was both surface and diffusion-controlled. Under manipulation by an external magnetic field, the sedimentation process of NPs@PAMAM@Fc was accelerated. Therefore, it may be possible that the obtained diffusion-controlled process was due to the increase in steric hindrance under magnetic field toward the diffusion of ions which served to maintain the electro-neutrality on the electrode surface during Fc oxidation. Indeed, the attracted NPs may stack on the electrode surface, thereby slowing down the diffusion of counter ions. In this case, the reaction will effectively be diffusion-limited, not by the diffusion of NPs that are immobilized on the surface, but by the diffusion of these counter ions. Another possibility that will be investigated in the future will be the influence of the formation of chain-like aggregates ('filaments') along the direction of the field [42,43]. Orientation of NPs filaments onto the working electrode surface depends on the magnetic field orientation. Therefore, filaments could be orthogonal or parallel to the working electrode surface. Both organizations may not lead to the same oxidation process for Fc molecules.

4. Conclusion

Electroactive magnetic NPs were prepared in a two-step process including the surface modification of initial magnetic NPs with PAMAM dendrimer and then the grafting of Fc onto the amine groups of PAMAM. Using complementary surface characterization techniques (colorimetric titration, zeta potential measurement and infrared spectroscopy), the successful grafting of PAMAM and Fc onto magnetic NPs was evidenced. After conjugation onto NPs, Fc underwent a redox potential shifting from 0.328 V to 0.590 V, which supports the covalent grafting of Fc carboxylic groups onto amine groups from PAMAM. A change from a reversible to an irreversible behaviour was also observed. The resulting NPs combined both redox and magnetic properties. The influence of an external magnetic field to attract NPs@PAMAM@Fc on the surface of working electrode was investigated on a microchip electrochemical device. Under magnetic attraction, electrochemical signal intensity was increased by a 2-fold factor for NPs@PAMAM@Fc with a decrease of detection limit compared to NPs freely dispersed in electrolyte. Electrochemical reaction of NPs@PAMAM@Fc was controlled by both surface and diffusion when dispersed in solution, while it was dominated by diffusion after magnetic attraction on the working electrode surface.

Acknowledgements

This work was supported by the BQR (‘Bonus Qualite´ Recherche’) of Ecole Centrale de Lyon. We are indebted to the Chinese Scholarship Council for the financial support of F. Chen.

References

[1] R. H. Kodama, *J. Magn. Magn. Mater.* **1999**, *200*, 359.

[2] S. Chikazumi, S. Taketomi, M. Ukita, M. Mizukami, H. Miyajima, M. Setogawa, Y. Kurihara, *J. Magn. Magn. Mater.* **1987**, *65*, 245.

[3] A. H. Lu, E. L. Salabas, F. Schüth, *Angew. Chem., Int. Ed.* **2007**, *46*, 1222.

[4] Y. C. Kim, S. Han, S. Hong, *Water Sci. Technol.* **2011**, *64*, 469.

[5] S. C. Tsang, V. Caps, I. Paraskevas, D. Chadwick, D. Thompsett, *Angew. Chem. Int. Ed.* **2004**, *43*, 5645.

[6] K. Hola, Z. Markova, G. Zoppellaro, J. Tucek, R. Zboril, *Biotechnol. Adv.* **2015**, *33*, 1162.

[7] R.-P. Liang, G.-H. Yao, L.-X. Fan, J.-D. Qiu, *Anal. Chim. Acta* **2012**, *737*, 22.

[8] A. Faucon, H. Benhelli-Mokrani, F. Fleury, L. Dubreil, P. Hulin, S. Nedellec, T. Doussineau, R. Antoine, T. Orlando, A. Lascialfari, J. Fresnais, L. Lartigue, E. Ishow, *J. Colloid Interface Sci.* **2016**, *479*, 139.

[9] H. Li, Q. Wei, J. He, T. Li, Y. Zhao, Y. Cai, B. Du, Z. Qian, M. Yang, *Biosens. Bioelectron.* **2011**, *26*, 3590.

[10] M. Trévisan, M. Schawaller, G. Quapil, E. Souteyrand, Y. Mérieux, J.-P. Cloarec, *Biosens. Bioelectron.* **2010**, *26*, 1631.

[11] J. R. McCarthy, R. Weissleder, *Adv. Drug Deliv. Rev.* **2008**, *60*, 1241.

[12] C. Liang, L. Jing, X. Shi, Y. Zhang, Y. Xian, *Electrochim. Acta* **2012**, *69*, 167.

[13] I. Willner, E. Katz, *Angew. Chem. Int. Ed.* **2003**, *42*, 4576.

[14] S. J. H. Soenen, U. Himmelreich, N. Nuytten, T. R. Pisanic, A. Ferrari, M. De Cuyper, *Small* **2010**, *6*, 2136.

[15] Y. Song, Y. Y. Huang, X. Liu, X. Zhang, M. Ferrari, L. Qin, *Trends Biotechnol.* **2014**, *32*, 132.

[16] Y. Xu, J. Xie, R. Chen, Y. Cao, Y. Ping, Q. Xu, W. Hu, D. Wu, L. Gu, H. Zhou, X. Chen, Z. Zhao, J. Zhong, R. Li, *Sci. Rep.* **2016**, *6*, 1.

[17] L. Fernández, H. Carrero, *Electrochim. Acta* **2005**, *50*, 1233.

[18] J. Qiu, H. Peng, R. Liang, *Electrochem. commun.* **2007**, *9*, 2734.

[19] J. D. Qiu, M. Xiong, R. P. Liang, H. P. Peng, F. Liu, *Biosens. Bioelectron.* **2009**, *24*, 2649.

[20] E. Çevik, M. Şenel, A. Baykal, M. F. Abasiyanik, *Curr. Appl. Phys.* **2013**, *13*, 1611.

[21] R. Peng, W. Zhang, Q. Ran, C. Liang, L. Jing, S. Ye, Y. Xian, *Langmuir* **2011**, *27*, 2910.

[22] J. P. Sęk, A. Kasprzak, M. Bystrzejewski, M. Poplawska, W. Kaszuwara, Z. Stojek, A. M. Nowicka, *Biosens. Bioelectron.* **2018**, *102*, 490.

[23] P. Tengvall, E. Jansson, A. Askendal, P. Thomsen, C. Gretzer, *Colloids Surfaces B Biointerfaces* **2003**, *28*, 261.

[24] G. T. Hermanson, A. Krishna Mallia, P. K. Smith, *Immobilized Affinity Ligand Techniques*, Academic Press, **1992**.

[25] F. Chen, N. Haddour, M. Frenea-Robin, Y. Chevolot, V. Monnier, *ChemistrySelect* **2018**, *3*, 2823.

[26] G. Coussot, E. Nicol, A. Commeyras, I. Desvignes, R. Pascal, O. Vandenabeele-Trambouze, *Polym. Int.* **2009**, *58*, 511.

[27] S. Schmidt, H. Wang, D. Pussak, S. Mosca, L. Hartmann, *Beilstein J. Org. Chem.* **2015**, *11*, 720.

[28] T. Wang, W.-L. Yang, Y. Hong, Y.-L. Hou, *Chem. Eng. J.* **2016**, *297*, 304.

[29] S. M. Batterjee, M. I. Marzouk, M. E. Aazab, M. A. El-Hashash, *Appl. Organomet. Chem.* **2003**, *17*, 291.

[30] C. M. Cardona, S. Mendoza, A. E. Kaifer, *Chem. Soc. Rev.* **2000**, *29*, 37.

[31] D. L. Stone, D. K. Smith, P. T. McGrail, *J. Am. Chem. Soc.* **2002**, *124*, 856.

[32] R. S. Kelly, "Analytical Electrochemistry: The Basic Concepts," can be found under http://www.asdlib.org/onlineArticles/ecourseware/Kelly_Potentiometry/EC_CONCEPTS1.HTM, **2009**.

[33] P. A. Christensen, A. Hamnett, *Techniques and Mechanisms in Electrochemistry*, Blackie Academic & Professional, Glasgow, **1994**.

[34] R. S. Nicholson, I. Shain, *Anal. Chem.* **1964**, *36*, 706.

[35] C. S. Lim, A. Ambrosi, Z. Sofer, M. Pumera, *Nanoscale* **2014**, *6*, 7391.

[36] C. Batchelor-Mcauley, R. G. Compton, *J. Electroanal. Chem.* **2012**, *669*, 73.

[37] C. Batchelor-Mcauley, E. Kätelhön, E. O. Barnes, R. G. Compton, E. Laborda, A. Molina, *ChemistryOpen* **2015**, *4*, 224.

[38] L. Fotouhi, M. Fatollahzadeh, M. M. Heravi, *Int. J. Electrochem. Soc.* **2012**, *7*, 3919.

[39] J. D. Qiu, W. M. Zhou, J. Guo, R. Wang, R. P. Liang, *Anal. Biochem.* **2009**, *385*, 264.

[40] J. D. Qiu, J. Guo, R. P. Liang, M. Xiong, *Electroanalysis* **2007**, *19*, 2335.

[41] L. Fang, B. Liu, L. Liu, Y. Li, K. Huang, Q. Zhang, *Sensors Actuators B Chem.* **2016**, *222*, 1096.

[42] N. Haddour, Y. Chevolot, M. Trévisan, E. Souteyrand, J.-P. Cloarec, *J. Mater. Chem.* **2010**, *20*, 8266.

[43] V. Du, N. Luciani, S. Richard, G. Mary, C. Gay, F. Mazuel, M. Reffay, P. Menasché, O. Agbulut, C. Wilhelm, *Nat. Commun.* **2017**, *8*, 400.